Studies on a Stellarator Reactor of the Helias Type: The Power Balance

C.D. Beidler, E. Harmeyer, J. Kisslinger
I. Ott, F. Rau, H. Wobig

IPP 2/318 June 1993

MAX-PLANCK-INSTITUT FÜR PLASMAPHYSIK

85748 GARCHING BEI MÜNCHEN

MAX-PLANCK-INSTITUT FÜR PLASMAPHYSIK

GARCHING BEI MÜNCHEN

Studies on a Stellarator Reactor of the Helias Type: The Power Balance

C.D. Beidler, E. Harmeyer, J. Kisslinger
I. Ott, F. Rau, H. Wobig

IPP 2/318 June 1993

Die nachstehende Arbeit wurde im Rahmen des Vertrages zwischen dem Max-Planck-Institut für Plasmaphysik und der Europäischen Atomgemeinschaft über die Zusammenarbeit auf dem Gebiet der Plasmaphysik durchgeführt.

Contents

Abstract

The power balance of a Helias reactor is analysed using empirical scaling laws which describe current stellarator experiments. Since neoclassical transport in Helias configurations is not prohibitive to ignition, anomalous transport determines the parameters of the ignited state. In the following study the plasma profiles are taken as given and the power balance with an external heating power is evaluated numerically. Three empirical scaling laws, LHD-scaling, Gyro-Bohm scaling and Lackner-Gottardi scaling are extrapolated to reactor parameters. Present experiments (Wendelstein 7-AS, ATF, Heliotron E and CHS) can be described by these scaling laws, in Wendelstein 7-AS preference is given to the Lackner-Gottardi scaling since confinement improves with increasing rotational transform. LHD scaling and Gyro-Bohm scaling do not satisfy the ignition conditions; an improvement of confinement is necessary. However, Lackner-Gottardi scaling meets the ignition condition and the operating window of the Helias reactor was found in the following regime: Major radius 20 m, average plasma radius 1.6 m, magnetic field 5 T, density $n(0) = 3 - 4 \times 10^{20}\mathrm{m}^{-3}$ and temperature $T(0) \approx 15 - 17$ keV. The fusion output power is 2.5-3.0 GW and the average value of β= 4-5%. This lies within the MHD-stability limits of a Helias configuration. The effects of various parameter variations on the power balance (isotope effect, α-particle content, major radius, magnetic field) are also investigated.

1 Introduction

Stellarator reactor studies have been undertaken since the beginning of stellarator research. The first studies of modular stellarator reactors [1][2] mainly concentrated on technical issues neglecting the limitations set by confinement and stability. In contrast to these early studies, the Helias configuration [3] offers the chance to develop a self-consistent reactor concept where the plasma losses, MHD stability limits and α-particle losses are not prohibitive to ignition.

The dimensions of the Helias reactor are mainly determined by the technical limits of the coil system and the necessary space for blanket and shield. The main parameters are: Major radius 20 m, average plasma radius 1.6 m, magnetic field on axis 5 T, rotational transform on axis 0.84, transform on the boundary $\approx$ 1.0. Details of the Helias reactor concept are described in [4]. The MHD-stability limit in a 5-period Helias configuration is expected to be $\bar{\beta}$ = 4-5 % and the neoclassical transport losses can be characterised by an effective helical ripple of 1-2%. This immediately poses the question of whether ignition is possible and, if so, if the fusion power is in the desired regime of $P = 2.5 - 3.0$ GW.

In former reactor studies the bootstrap current presented a problem since the alteration of the magnetic field and the rotational transform could have had negative effects on plasma confinement. In Helias configurations this issue has been successfully addressed; the proper choice of the magnetic field nearly eliminates the bootstrap effect. The relevance of neoclassical theory to bootstrap effects has been demonstrated in the ATF [5] and Wendelstein 7-AS experiments [6]. With respect to confinement the situation is less satisfying. Since the neoclassical losses can be ruled out as a limiting factor, anomalous transport determines the power balance and thus the ignition condition. Various scaling laws of anomalous confinement (LHD scaling, Gyro-Bohm scaling, Lackner-Gottardi scaling [7]) have been tested in present-day stellarator experiments, showing no clear distinction among the various scaling laws. In Wendelstein 7-AS all three scaling laws fit the experimental data. Only future larger stellarator experiments can provide a relevant data base to establish reliable empirical scaling laws of plasma confinement. Therefore, the pragmatic approach is to extrapolate the empirical scaling laws to a reactor plasma and to test the ignition conditions under various assumptions on anomalous confinement.

In conventional stellarators prompt losses of α-particles lead to a strong reduction of heating power and to localised power deposition on the plasma facing components on the wall. In Helias configurations these losses can be strongly reduced by the poloidal magnetic drift of trapped α-particles, which increases with rising plasma pressure [8]. Although absolute confinement of all particle orbits is not possible in a 3-dimensional stellarator configuration, highly energetic α-particles can be confined over one slowing down time which is enough to neglect the effect of these losses on the power balance.

A rigorous power balance calculation would start from a transport code and calculate temperature and density profiles provided the transport coefficients, the boundary conditions and the radiative phenomena are given. However, too many effects are unknown to obtain reliable results from this procedure; therefore we follow the standard approach with fixed plasma profiles and empirical scaling laws for the confinement time. The plasma profiles are modelled analytically and the power balance is evaluated numerically.

A Helias reactor is a steady-state reactor with a low amount of recirculating power. To maintain the auxiliary systems roughly 10% of the electric power is needed. A rough power balance starting from an electric power of 1000 MW shows that on the plasma side a neutron power of 2000 - 2400 MW has to be delivered; this corresponds to an α-particle heating power of 500 - 600 MW. This figure sets a lower limit on the reactor performance and therefore determines strongly the dimensions and the plasma parameters of a Helias reactor. These relations are sketched in Fig. 1.

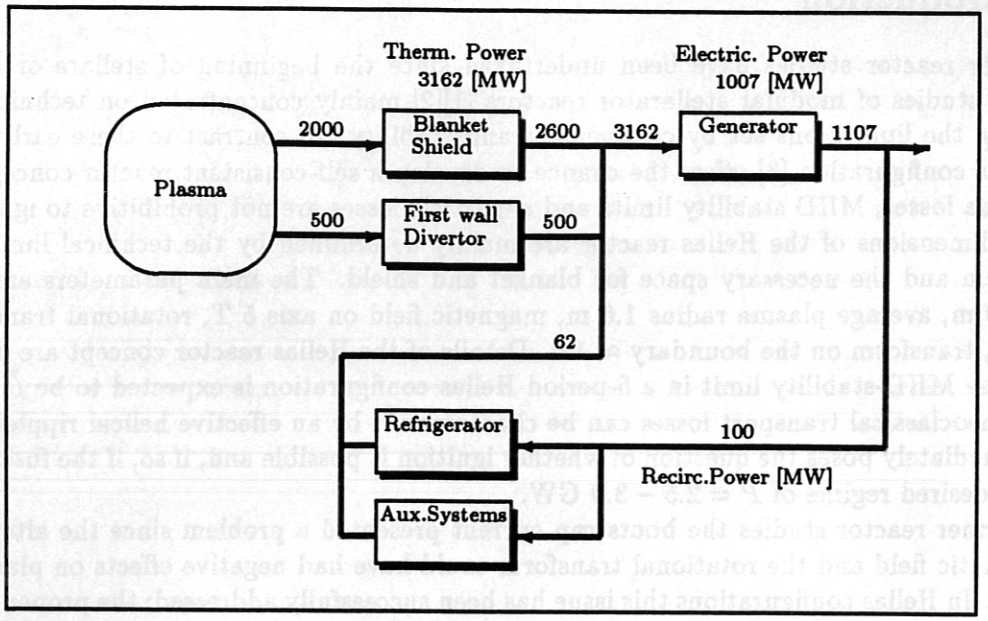

Figure 1: *Power flow diagram of a Helias reactor with α-particle heating power 500 MW, fusion power 2500 MW, blanket multiplication factor 1.3, thermal power 3162 MW, efficiency of generator 0.35, recirculating power 100 MW.*

2 Transport in the Helias Reactor

2.1 The Magnetic Field Configuration

The Helias reactor HSR is a scaled-up version of the magnetic field configuration envisaged for the Wendelstein 7-X experiment [9]. The 5-period Helias configuration has an aspect ratio of 12 and a magnetic well of $\delta V'/V' \approx -1\%$. The MHD-stability limit is determined by the ideal ballooning mode and is expected at $\bar{\beta} = 4 - 5\%$. With a smaller number of field periods one could lower the aspect ratio, however the stability limit would also decrease. On the other hand, a fusion power output of ≈ 3 GW requires a plasma $\bar{\beta}$ of $\approx 5\%$. In contrast to the reference configuration of Wendelstein 7-X, the reactor version HSR has a higher magnetic mirror on the axis ($\delta B/2B \approx 10\%$). This leads to a localisation of highly energetic α-particles within one field period and to a strong reduction of prompt losses of these particles. This effect and the poloidal magnetic drift which increases with rising plasma pressure are the reasons for the improved confinement of highly energetic α-particles in Helias configurations.

Pfirsch-Schlüter currents in Helias configurations are strongly reduced. In HSR the parallel equilibrium currents are smaller than the diamagnetic currents ($|j_{\|}| \leq 0.7|j_{\perp}|$). Therefore, a small Shafranov shift is to be expected. In Wendelstein 7-AS this prediction has been confirmed; the Shafranov shift has been reduced by a factor 2 in comparison with the ℓ=2 stellarator Wendelstein 7-A. Numerical calculations using the KW-code [10] showed a Shafranov shift of 9 - 13 cm in Wendelstein 7-X at $\bar{\beta} = 4\%$. Extrapolating this result to HSR (average plasma radius 1.6 m) yields a Shafranov shift of 27 - 40 cm at the same β. Without this reduction of Pfirsch-Schlüter currents a shift of more than 1 m would occur.

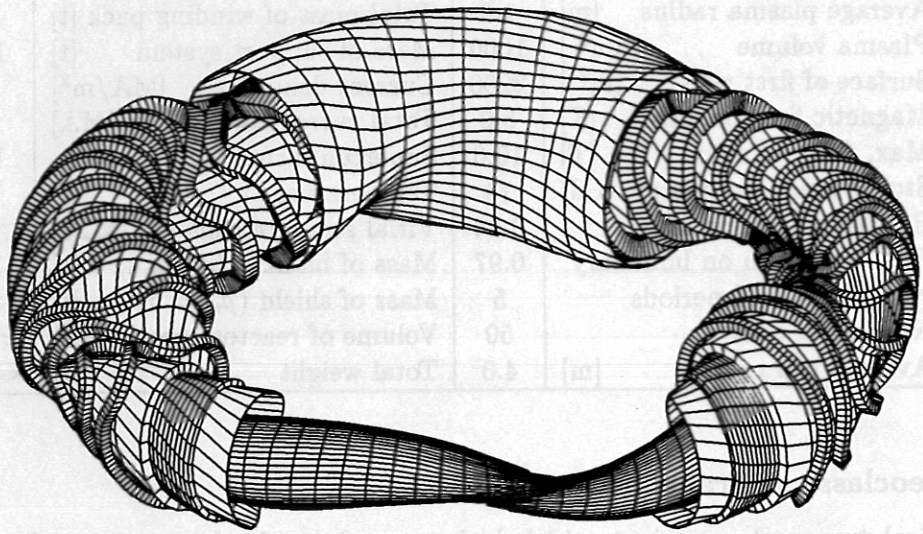

Figure 2: *Main components of a Helias reactor. In the foreground area magnetic surface, the first wall, blanket and shield. These are followed by coils with and without casing. The cryostat in the background. The dimensions are listed in Table I.*

To determine the dimensions of the reactor the following conditions and criteria have been imposed.

- The magnetic field is a 5-period Helias configuration. The magnetic field on axis is limited to 5 T, which allows one to stay within the present-day NbTi-technology.
- Sufficient space for shield, blanket and divertor systems must be provided. This requires a distance of at least 1.1 m between the first wall and coil winding pack.
- The coil system consists of one set of modular coils. Extra coils, as used in the experiments W7–AS and W7–X for parameter scanning, are not necessary.
- Since the confinement time scales roughly with the plasma volume the minimum size is also determined by the ignition condition.

These conditions lead to minimum reactor dimensions listed in Table I. The dominating criterion is the necessity to provide sufficient space for blanket and shield; the available space for the components is 1.1 m at the narrowest position on the inboard side. The parameters of the reference reactor listed in table I are the basis of the power balance discussed in this paper. Several other versions with 10% larger dimensions in major and minor radius have also been investigated for comparison. The increase of the magnetic field by 10% provides better confinement which improves the ignition condition appreciably. The plasma parameters which result from these dimensions and the envisaged confinement properties are listed in table II. In this regime the fusion power of the Helias reactor ranges between 2.5 and 3.8 GW. Details of the coil system are described elsewhere [11].

In the following sections the transport properties of the Helias configuration will be investigated.

Table I: Data of the Helias reactor

Average major radius	[m]	20	Volume of coil wdg. pack	[m^3]	12.0
Average plasma radius	[m]	1.6	Total mass of winding pack	[t]	3800
Plasma volume	[m^3]	1000	Mass of support system	[t]	10400
Surface of first wall	[m^2]	2200	Current density	[MA/m^2]	25.0
Magnetic field on axis	[T]	5.0	Total current in coil	[MA]	10.7
Max. field on coils	[T]	10.6	Superconductor		NbTi
Stored magnetic energy	[GJ]	74	Temperature	[K]	1.8
Rot. transform on axis		0.84	Virial stress in coils	[MPa]	122
Rot. transform on boundary		0.97	Mass of blanket ($\rho_m = 4$)	[t]	3300
Number of field periods		5	Mass of shield ($\rho_m = 5$)	[t]	8360
Number of coils		50	Volume of reactor core	[m^3]	$\approx 10^4$
Average coil radius	[m]	4.0	Total weight	[t]	≈25800

2.2 Neoclassical Transport

Neoclassical transport rates in toroidal devices are determined most conveniently through a knowledge of the magnitude of the magnetic field expressed in flux coordinates

$$\frac{B}{B_0} = 1 + \sum_{m,\ell} C_{m,\ell}(r) \cos mp\phi \cos \ell\theta + \sum_{m,\ell} S_{m,\ell}(r) \sin mp\phi \sin \ell\theta. \qquad (1)$$

In this expression r is a flux surface label, related to the toroidal flux through the expression $\psi = B_0 r^2/2$, ϕ and θ are toroidal and poloidal angle-like variables, respectively, and p is the field period number; the radial dependences of the largest harmonics for the Helias reactor, HSR, are illustrated in Figure 3. Numerical methods such as Monte Carlo simulations [12] and the DKES (Drift-Kinetic Equation Solver) code [13] have been developed to calculate neoclassical transport coefficients in such arbitrarily complex magnetic fields. Results obtained in this manner are the most accurate currently available but have the drawback that they require a good deal of computer time. A considerable simplification is made possible by noting in Figure 3 that the $m = 0$ and $m = 1$ harmonics predominate in the magnetic field spectrum (this is true for the majority of stellarator-type devices) and encorporating only these harmonics in an analytic theory of stellarator transport based on the solution of a "ripple-averaged" kinetic equation [14]. Scaling studies then lead to approximate expressions for the particle and heat fluxes which are valid in all reactor-relevant regimes

$$\begin{bmatrix} \Gamma_j \\ Q_j \end{bmatrix} = -\frac{2}{\sqrt{\pi}} n_j \int_0^\infty dx_j \begin{bmatrix} x_j^{1/2} \\ (eT_j)\, x_j^{3/2} \end{bmatrix} D(x_j)\, e^{-x_j} \left\{ \frac{n_j'}{n_j} + \frac{q_j \Phi'}{eT_j} + \left(x_j - \frac{3}{2}\right) \frac{T_j'}{T_j} \right\} \qquad (2)$$

(where column vectors have been employed for notational convenience). Here n_j is the density of particle species j, T_j is its temperature in eV and q_j its charge, e is the elementary charge, Φ the electrostatic potential (assumed to be only a function of r) and a prime denotes $\partial/\partial r$. The thermal velocity of particle species j is given by $v_j = (2eT_j/m_j)^{1/2}$ where m_j is the particle's mass, so that

$$x_j = \frac{m_j v^2}{2eT_j} = \frac{v^2}{v_j^2}\,.$$

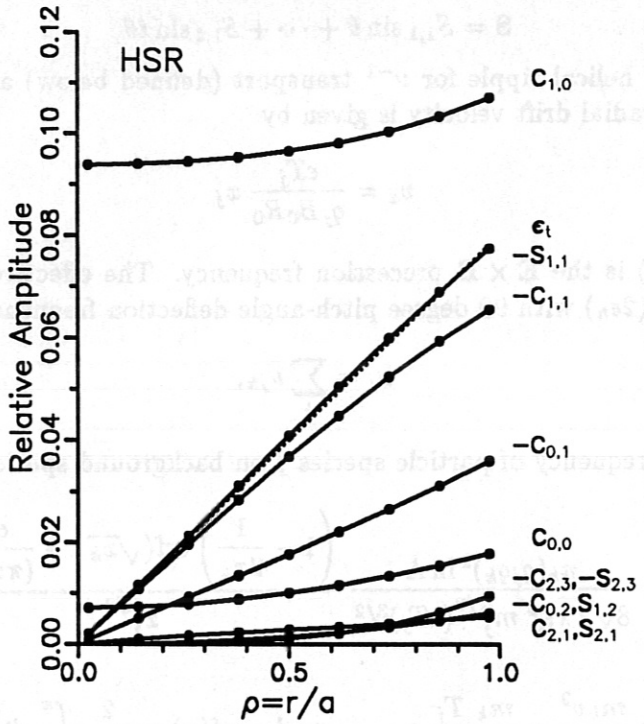

Figure 3: *Coefficients of the harmonics of B according to the decomposition given in Equation (1) are shown as a function of normalized plasma minor radius for the Helias reactor, HSR; the inverse aspect ratio, $\epsilon_t \equiv r/R_0$, is shown by the dotted line (roughly coinciding with the $-S_{1,1}$ curve). Note that $|C_{0,1}|/\epsilon_t \approx 0.45$ for HSR.*

The *monoenergetic* diffusion coefficient, $D(x_j) = D_h(x_j) + D_a(x_j)$, is taken to be a sum of terms describing: (a) the transport due to processes associated with particles trapped in the stellarator's helical ripples

$$D_h(x_j) = \frac{\frac{4}{9\pi}(2\epsilon_h)^{1/2}\,\nu_{eff}\left(v_d\frac{C_{0,1}}{\epsilon_t}\right)^2}{\left(\frac{\epsilon_h}{\epsilon_{eff}}\right)^{3/2}\left(\nu_{eff}\frac{C_{0,1}}{\epsilon_t}\right)^2 + (\nu_{eff}|\Omega_E|^3)^{1/2} + 4\frac{|C_{0,1}|}{\epsilon_h}\Omega_E^2} \tag{3}$$

and, (b) the transport expected in an axisymmetric device of inverse aspect ratio $\epsilon_t = r/R_0$, rotational transform ι, and toroidal modulation of the magnetic field $|C_{0,1}|$,

$$D_a(x_j) = \frac{\left(\frac{C_{0,1}}{\epsilon_t}\right)^2\frac{v_d}{\Omega\iota}}{\frac{3}{v_j x_j^{1/2}} + \frac{\iota|C_{0,1}|^{3/2}}{R_0\nu_j}} + \frac{7}{5}\left(\frac{C_{0,1}}{\epsilon_t}\right)^2\frac{v_d R_0}{\Omega\iota^2}\,\nu_j\,. \tag{4}$$

In these expressions the magnitude of the helical ripple has been determined from the $m = 1$ harmonics according to

$$\epsilon_h = \frac{1}{2\pi}\int_0^{2\pi} d\theta\,(\mathbf{C}^2 + \mathbf{S}^2)^{1/2}\,,$$

$$\mathbf{C} = C_{1,0} + C_{1,1}\cos\theta + \cdots + C_{1,\ell}\cos\ell\theta,$$

$$\mathbf{S} = S_{1,1}\sin\theta + \cdots + S_{1,\ell}\sin\ell\theta,$$

ϵ_{eff} is the "effective" helical ripple for ν^{-1} transport (defined below) and $\Omega = q_j B/m_j$ is the gyro frequency. The radial drift velocity is given by

$$v_d = \frac{eT_j}{q_j B_0 R_0}\, x_j$$

and $\Omega_E = -\Phi'/(rB_0)$ is the $\mathbf{E}\times\mathbf{B}$ precession frequency. The effective collision frequency is defined by $\nu_{eff} = \nu_j/(2\epsilon_h)$ with 90 degree pitch-angle deflection frequency

$$\nu_j = \sum_k \nu_{jk},$$

where the deflection frequency of particle species j on background species k is given by

$$\nu_{jk} = \frac{n_k (q_j q_k)^2 \ln\Lambda}{8\sqrt{2}\,\pi\epsilon_0^2\, m_j^{1/2} (eT_j)^{3/2}} \frac{\left(1 - \dfrac{1}{2x_k}\right)\mathrm{erf}(\sqrt{x_k}) + \dfrac{e^{-x_k}}{(\pi x_k)^{1/2}}}{x_j^{3/2}}$$

with

$$x_k = \frac{m_k v^2}{2eT_k} = \frac{m_k}{T_k}\frac{T_j}{m_j}\, x_j, \qquad \text{and} \quad \mathrm{erf}(x) = \frac{2}{\sqrt{\pi}}\int_0^x dt\, e^{-t^2},$$

and where $\ln\Lambda$ is the Coulomb Logarithm and ϵ_0 is the permittivity of free space. Unless otherwise noted, all quantities have been expressed in mks units (note, however, that eT_j has units of energy). $D(x_j)$ earns the name monoenergetic diffusion coefficient since it is appropriate for direct comparison with the results of Monte Carlo simulations in which groups of monoenergetic test particles of a given x_j experience only pitch-angle scattering in the course of their simulation. It has been constructed so as to smoothly reproduce the results of the scaling studies and results known from analytic theory. For example, the ν^{-1} regime $D_h \approx (4/9\pi)(2\epsilon_{eff})^{3/2} v_d^2/\nu_j$ is obtained from Equation 3 for large values of ν_{eff}, while the plateau result $D_a \approx (C_{0,1}/\epsilon_t)^2 (v_d v/3\Omega\iota)$ is recovered from Equation 4 for intermediate values of ν_j. In the former case, ϵ_{eff} has been formulated so that the neoclassical losses in any arbitrarily complex stellarator magnetic field are equivalent to those in the model field

$$B/B_0 = 1 - \epsilon_t\cos\theta - \epsilon_{eff}\cos(L\theta - p\phi). \tag{5}$$

Typically, Helias configurations exhibit a high degree of transport optimization; for the Helias reactor HSR, $\epsilon_{eff}(r) \lesssim 0.025$ even though $\epsilon_h(r) > 0.09$ (note that ϵ_h is large across the entire plasma cross-section for HSR due to the large mirror term, $C_{1,0}$). Equations 3 and 4 also reflect the significant reduction of the neoclassical transport in Helias configurations where the toroidal modulation of B is small with respect to ϵ_t (see Figure 3); diffusion coefficients are reduced in all regimes by the factor $(C_{0,1}/\epsilon_t)^2$, with the exception of the banana regime where the factor is $(|C_{0,1}|/\epsilon_t)^{1/2}$ and the ν regime where the factor is $|C_{0,1}|/\epsilon_t$ (this effect has already been accounted for in the formulation of ϵ_{eff} so that this reduction factor does not appear explicitly in the ν^{-1} result).

The validity of these analytic expressions may be verified by use of Monte Carlo simulations; an example is given in Figure 4. In all cases the simulation plasmas have been assumed to be composed of deuterons, tritons and electrons (with species indicies $j = D, T, e$, respectively) with $T_D = T_T = T_e = 10$ keV and $2n_D = 2n_T = n_e$. Test particles were either deuterons or electrons with $x_j = 1$ at their launch surface $\rho = 0.5$; the test particles experienced only pitch-angle

scattering in the course of their simulation. An electrostatic potential of the form $\Phi = \Phi_0(1-\rho^2)$ was assumed to be present in the plasma; results are presented here for $\Phi_0 = -15,000$ V (the solid lines and solid circles in Figure 4) and for $\Phi_0 = 0$ (dotted lines and open circles). (The Monte Carlo results for $\Phi_0 = 0$ determine the value of the effective helical ripple, $\epsilon_{eff} = 0.019$.) Device parameters used in the simulation can be found in Table I; the magnetic field is composed of the harmonics given in Figure 3.

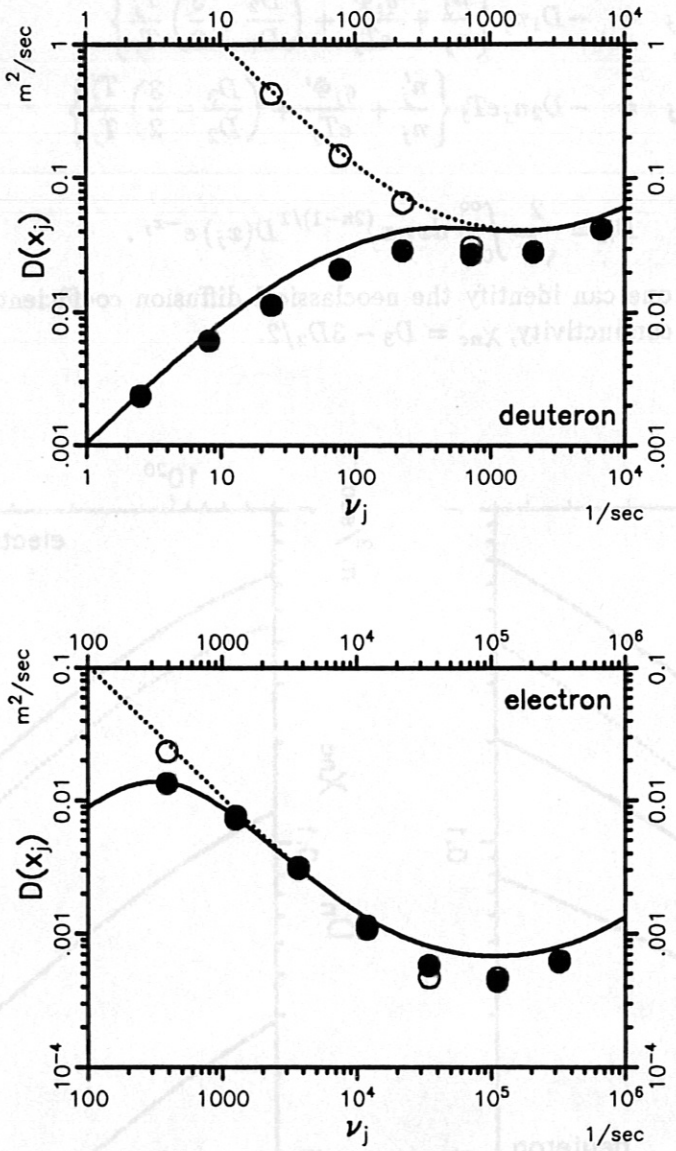

Figure 4: *Results from the analytic expression for the monoenergetic diffusion coefficient, $D = D_h + D_a$, are compared with those of Monte Carlo simulations for the Helias reactor HSR at $\rho = 0.5$. Analytic results are shown by the solid lines for $\Phi/T_j = -9/8$ and by dotted lines for $\Phi/T_j = 0$; the corresponding Monte Carlo results are given by solid circles and open circles, respectively. Test particles were either deuterons (top) or electrons (bottom) with $x_j = 1$; the background particles species were assumed to have the temperatures $T_D = T_T = T_e = 10$ keV. The collision frequency, ν_j, was varied by changing the density of the simulation plasma, subject to the condition $2n_D = 2n_T = n_e$.*

For the results shown in Figure 4, ν_j has been varied by changing the plasma density; a typical operational density for a Helias reactor of $2n_D = 2n_T = n_e = 2 \times 10^{20}$ m^{-3} yields $\nu_D \approx 165$ sec^{-1} and $\nu_e \approx 23,700$ sec^{-1}, values which are roughly at the center of their respective ν_j axes in Figure 4. The accuracy of the analytic curves, demonstrated by the results presented in Figure 4, allows one to determine neoclassical transport coefficients much more rapidly then would be possible using a numerical approach. A convenient method for doing so is to cast the equations for the particle and heat fluxes into the form [12]

$$\begin{aligned} \Gamma_j &= -D_1 n_j \left\{ \frac{n_j'}{n_j} + \frac{q_j \Phi'}{eT_j} + \left(\frac{D_2}{D_1} - \frac{3}{2} \right) \frac{T_j'}{T_j} \right\} \\ Q_j &= -D_2 n_j e T_j \left\{ \frac{n_j'}{n_j} + \frac{q_j \Phi'}{eT_j} + \left(\frac{D_3}{D_2} - \frac{3}{2} \right) \frac{T_j'}{T_j} \right\} \end{aligned} \tag{6}$$

where

$$D_n = \frac{2}{\sqrt{\pi}} \int_0^\infty dx_j \, x_j^{(2n-1)/2} D(x_j) \, e^{-x_j} \, . \tag{7}$$

From these expressions, one can identify the neoclassical diffusion coefficient, $D_{nc} = D_1$, and the neoclassical thermal conductivity, $\chi_{nc} = D_3 - 3D_2/2$.

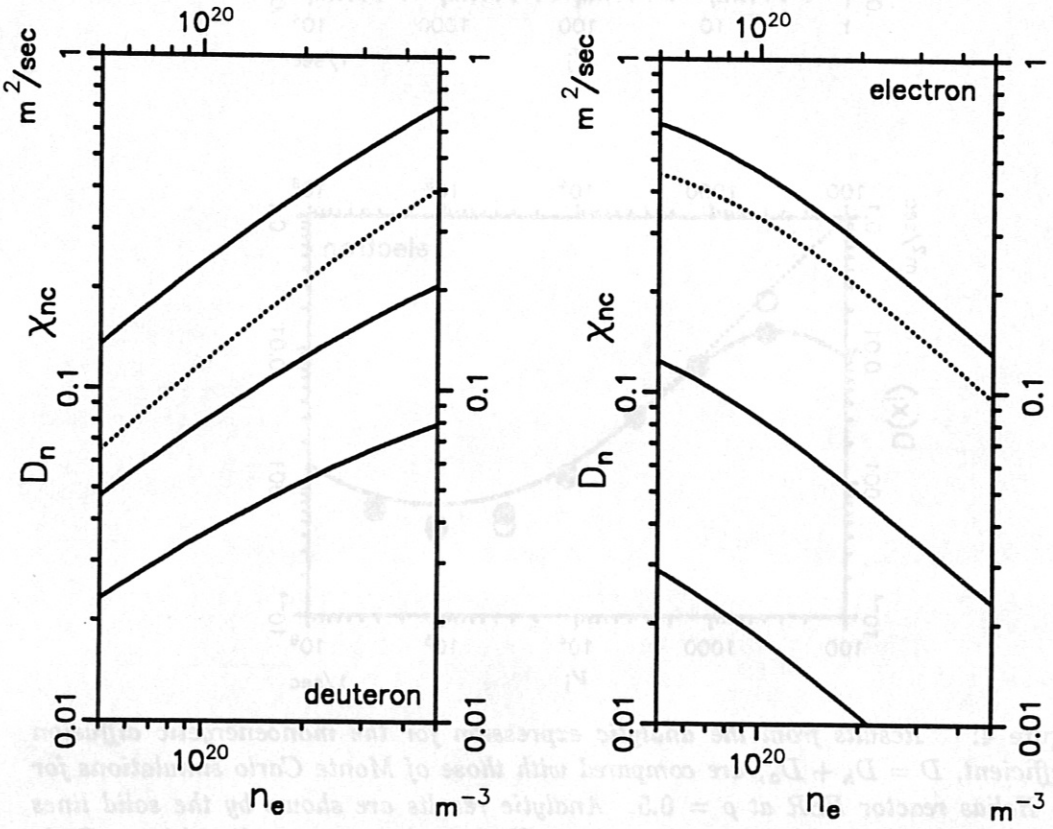

Figure 5: *The D_1, D_2, D_3 (solid lines from bottom to top, respectively) and χ_{nc} (dotted line) curves are plotted for HSR parameters for both deuterons (left) and electrons (right) over the range of densities $5 \times 10^{19} \leq n_e \leq 5 \times 10^{20}$ for the $\rho = 0.5$ flux surface. It has once again been assumed that $2n_D = 2n_T = n_e$, $T_D = T_T = T_e = 10$ keV and that $\Phi/T_j = -9/8$.*

An example of the use of these formulas for HSR is given in Figure 5; the D_1, D_2, D_3 (solid lines from bottom to top, respectively) and χ_{nc} (dotted line) curves are plotted for both deuterons and electrons over the range of possible operational densities $5 \times 10^{19} \leq n_e \leq 5 \times 10^{20}$ for the $\rho = 0.5$ flux surface. It has once again been assumed that $2n_D = 2n_T = n_e$ and that $T_D = T_T = T_e = 10$ keV. The electrostatic potential has the form $\Phi = -15,000(1 - \rho^2)$ so that $\Phi/T_j = -9/8$, a value which lies at the conservative end of the range $-2 \lesssim \Phi/T_j \lesssim -1$, a range of values which has been determined for HSR from the ambipolarity constraint, $\Gamma_e = \Gamma_D + \Gamma_T$ (for realistic plasma parameters and profiles only the so-called ion root is present in HSR). As Figure 5 illustrates, a potential of this magnitude is sufficient to "suppress" the ν^{-1} regime for ionic species but has essentially no effect on the electrons.

An approximate rule of thumb for maintaining a burning plasma is that the total thermal conductivity must satisfy $\chi \lesssim 1$ (see below) where χ includes both neoclassical and anomalous losses. Since the anomalous thermal conductivity by itself may approach this value, it is clearly necessary that $\chi_{nc} \ll 1$. Referring to Figure 5, one sees that this condition is indeed fulfilled in HSR for typical operational densities; for $n_e = 2 \times 10^{20}$ m^{-3} the neoclassical thermal conductivity of both deuterons and electrons is $\chi_{nc} \approx 0.2$ m^2/sec. Thus, the neoclassical losses in an ignited Helias reactor may often be ignored with respect to the anomalous losses when determining the power balance of the reactor, a situation which is quite different from that of reactor concepts based on conventional stellarator-type devices.

2.3 Anomalous Transport

Anomalous transport is a phenomenon found in all present-day stellarator experiments. Since the underlying physical mechanisms are unknown, extrapolations to future experiments and the stellarator reactor are rather uncertain and subject to large errors. Nevertheless, empirical scaling laws found in stellarator experiments will be extended to reactor conditions in order to test the ignition conditions and to identify those parameters which have strong influence on the ignited state.

Tokamak scaling laws often depend on the plasma current as an independent parameter which prevents a naive extrapolation to currentless stellarator discharges. To replace the current by the corresponding rotational transform is common practice, however a rigorous justification is not yet available and in stellarator configurations with large shear the problem arises which value of ι is the relevant one. The Lackner-Gottardi scaling [7] which was originally derived for tokamak discharges can be understood on the basis of a random walk process with the banana width Δ of trapped particles as the elementary step width and the bounce frequency ω_b as the characteristic frequency. Let f_t be the number of trapped particles; then the transport coefficient of this random walk process is $D \propto f_t \omega_b \Delta^2$. The confinement time following this sort of reasoning would be $\tau_E \propto Ra^2 B^{0.8} \bar{n}^{0.6} P^{-0.6} \iota^{0.4}$. Since the key element in this process is the banana orbit which is related to the poloidal field B_θ the scaling can also be applied to stellarators taking into account the equation of the banana orbits. This empirical scaling law which also fits the experimental data in Wendelstein 7-AS is

$$\tau_E = 0.175 Ra^2 B^{0.8} \bar{n}^{0.6} P^{-0.6} \iota^{0.4} \left(\frac{A}{1.5}\right)^{0.5}. \tag{8}$$

The units are: time in s, heating power P in MW, magnetic field B in T, line average density $\bar{n}$ in 10^{20} m^{-3}, major radius R and average plasma radius a in m. The isotope effect, described by the atomic number A, has not yet been verified in stellarator experiments, however, since this effect has been found in many tokamak experiments, it will be included tentatively to test its relevance for reactor conditions.

Since the banana orbit is the elementary step in the random walk process of anomalous transport it may be expected that in Helias configurations, where due to the optimisation

procedure the deviation of trapped particles from magnetic surfaces is appreciably smaller than in tokamaks or conventional stellarators, the anomalous transport is also reduced by this effect. The connection length or length of a banana orbit in tokamaks is $L_c = R/\iota$; in a Helias configuration with quasi-helical symmetry this length is roughly $L_c \approx R/|\iota - p|$. p is the number of field periods. In the Helias reactor the choice is $p = 5$. Because of the shorter connection length the bounce frequency increases and the banana width decreases. The anomalous transport coefficient scales with $|\iota - p|^{-1}$ and the confinement time with $|\iota - p|^{0.4}$. Therefore, in the confinement time in Eq. 8 the factor $\iota^{0.4}$ has to be replaced by $|\iota - p|^{0.4}$. In the configuration HSR envisaged for the Helias reactor, the particle orbits are more complicated than those in the more symmetric quasi-helical cases. Trapped particles remain in one field period and precess poloidal direction. The configuration looks more like a linked mirror configuration than a quasi-helical configuration. Since the radial width of the banana orbits is as small as in the quasi-helical case it has to be expected that also the arguments concerning the radial transport given above remain valid.

Besides the Lackner-Gottardi scaling, the LHD scaling and the Gyro-Bohm scaling are employed to predict plasma parameters in HSR. The LHD-scaling is

$$\tau_E = 0.17 R^{0.75} a^2 B^{0.84} \bar{n}^{0.69} P^{-0.58} \left(\frac{A}{1.5}\right)^{0.5}. \tag{9}$$

and the Gyro-Bohm scaling

$$\tau_E = 0.25 R^{0.6} a^{2.2} B^{0.8} \bar{n}^{0.6} P^{-0.68} \left(\frac{A}{1.5}\right)^{0.5}. \tag{10}$$

These two scaling laws do not show a dependence on the rotational transform, however a positive scaling with ι ($\tau_E \propto \iota^{0.23}$) was found in Wendelstein 7-AS [15] supporting the Lackner-Gottardi type scaling. As mentioned above the isotope factor has not yet been verified in stellarator experiments. Therefore two cases are considered: one with $A = 1.5$ which neglects the isotope effect and a second with $A = 2.5$. Experiments in the ATF torsatron can be described by Gyro-Bohm scaling , however, it should be noted that— except for the factor $\iota^{0.4}$ — there is almost no difference between LG scaling and Gyro-Bohm scaling. Since ATF and W 7-AS have the same major radius the R-dependence cannot be checked.

Theoretical effort to explain anomalous transport in stellarators have not led to a satisfying result. The close relationship of anomalous transport in stellarators and tokamaks rules out the toroidal plasma current as the driving mechanism. Resistive interchange instabilities are favoured to explain anomalous transport in torsatrons , whereas W 7-A and W 7-AS are stable against resistive interchange modes but unstable against resistive ballooning modes . In the reactor regime, resistive effects will be restricted to the boundary region; the bulk of the plasma is in the low-collisionality regime. Here, particle orbits play a decisive role in exciting instabilities and in the stochastic diffusion caused by fluctuating fields.

3 Power Balance

3.1 Alpha-particles in the Helias reactor

Since highly energetic α-particles are the only energy source in the plasma the behaviour of these particles plays a decisive role in the power balance of the reactor. In fact, there are three different reasons why α-particle confinement in a Helias reactor is of great importance. In stellarators highly energetic particles trapped in local magnetic wells may drift to the wall and cause local damage to the first wall material. This usually happens in a time short compared with the slowing down time and therefore also diminishes the the available heating power for the plasma. Thirdly, after slowing down, good confinement of the thermal α-particles favours ash accumulation and thus has a negative effect on the power balance.

In the Helias reactor some effort has been made to overcome these difficulties. Firstly, due to the high density and low temperature of the burning plasma the slowing down time is on the order of 0.1 s, and therefore the confinement time of energetic α-particles need not be larger than 0.1 s. Although there is no absolute confinement of trapped particles in a configuration without symmetry, improved confinement of these particles in a Helias reactor can be achieved by localizing the trapped particles in one field period and by utilizing the poloidal magnetic drift to avoid the formation of superbanana orbits. That this method is indeed effective has been demonstrated numerically by Lotz et al.[8]. The result is that nearly all highly energetic α-particles are confined for one slowing down time if the plasma β is sufficiently large. The poloidal magnetic drift already becomes effective at $\bar{\beta} = 2\%$. In view of this result, prompt losses of α-particles have been neglected in the power balance.

This favourable picture may be overshadowed by the excitation of global Alfvén modes by the α-particles and the subsequent loss of α- particles. The excitation mechanism will not differ from the mechanism in tokamaks, however, the spectrum of the GAE's will be different because of the difference in the ι-profile and the Fourier spectrum of the magnetic field. Furthermore, given a spectrum of Alfvén eigenmodes, the induced diffusion of particles depends on resonance conditions and the overlap of islands in the particle orbits. Mynick [17] has investigated this phenomenon in tokamak geometry showing that above an amplitude of $\delta B_r/B = 10^{-3}$ island overlap and stochastic diffusion leads to a large loss fraction of α-particles. Here, the difference in the ι-profile may be of importance. Drift-optimization of the passing particles and the small shear of the magnetic field also leads to a small shear of the drift orbits. Although small shear in the drift orbits enhances the island size, resonance overlap and stochastisation is reduced because of the wider spacing of the resonance lines. Numerical calculations are in preparation to study this effect in Helias geometry.

The third critical issue in α-particle physics is the confinement of thermal particles. Here, the neoclassical losses by trapped particles may be beneficial in reducing the fraction of thermal α's. The neoclassical confinement time of 200 KeV particles in the Helias reactor is around 6 s and the confinement time of thermal particles around 15 s. These numbers are less than 10 energy confinement times. If particle transport is anomalous this should also affect the thermal α's and reduce the confinement time to a lower level. A confinement time of less than 10 energy confinement times is compatible with the exhaust condition and the assumed concentration of the thermal α-particles [18] In the following we consider the concentration of thermal α- particles as a free parameter ($f_\alpha \leq 10\%$); a more self-consistant treatment requires the knowledge of the exact α-particle confinement and its dependence on the plasma parameters.

3.2 Plasma Profiles

A realistic prediction of the plasma parameters in a Helias reactor requires knowledge of transport processes and radiation losses of the fusion plasma close to the MHD-stability limit. Since reliable information about these processes is not available, a more reasonable procedure is to postulate the parameters of an attractive stellarator reactor and check whether phenomena known from theory and experiment meet the requirements of the stellarator reactor. Instead of calculating plasma parameters of an ignited state using a transport code, we specify the plasma profiles and investigate the power balance between α-particle heating, radiation losses and conductive losses. In modelling the plasma parameters, we assume equal temperature for ions and electrons and choose the following form for the profiles

$$T(r) = \frac{T(0)}{1+(r/r_T)^{2\alpha_T}} \quad ; \quad n(r) = \frac{n(0)}{1+(r/r_n)^{2\alpha_n}} \tag{11}$$

with $0 \leq r \leq 1$. r is the average radius of the magnetic surface normalised to the radius of the last surface. This average radius is defined by the volume of the magnetic surface $V(r) = 2\pi^2 R a^2 r^2$. The parameter set $r_T, \alpha_T, r_n, \alpha_n$ characterises the shape of the profiles; two cases will be analysed in the following:

- case 1: $r_T = 0.625$, $\alpha_T = 2.0$, $r_n = 0.6$, $\alpha_n = 3.0$
- case 2: $r_T = 0.525$, $\alpha_T = 1.5$, $r_n = 0.75$, $\alpha_n = 5.0$

These profiles are shown in Figure 6.

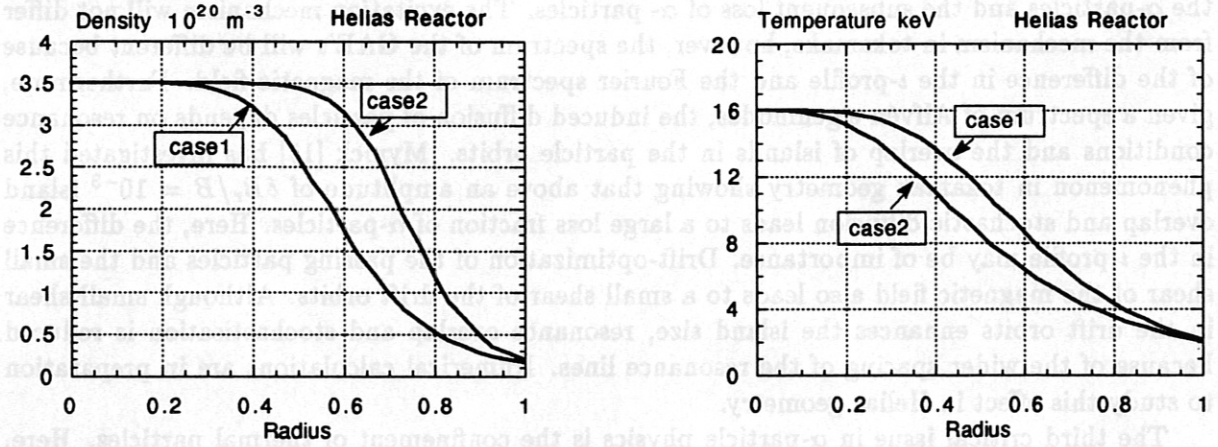

Figure 6: *Left: Density profiles, right: Temperature profiles*

The profiles in case 1 yield a higher α-power than those in case 2, however the pressure gradient is steeper than in case 2 and therefore a lower stability limit has to be expected. Case 2 has been optimised with respect to the pressure gradient, for the reason of MHD stability the pressure gradient has been chosen as small as possible. This choice of the profiles leads to a more peaked α-heating as can be seen from the profiles exhibited in Figure 7.

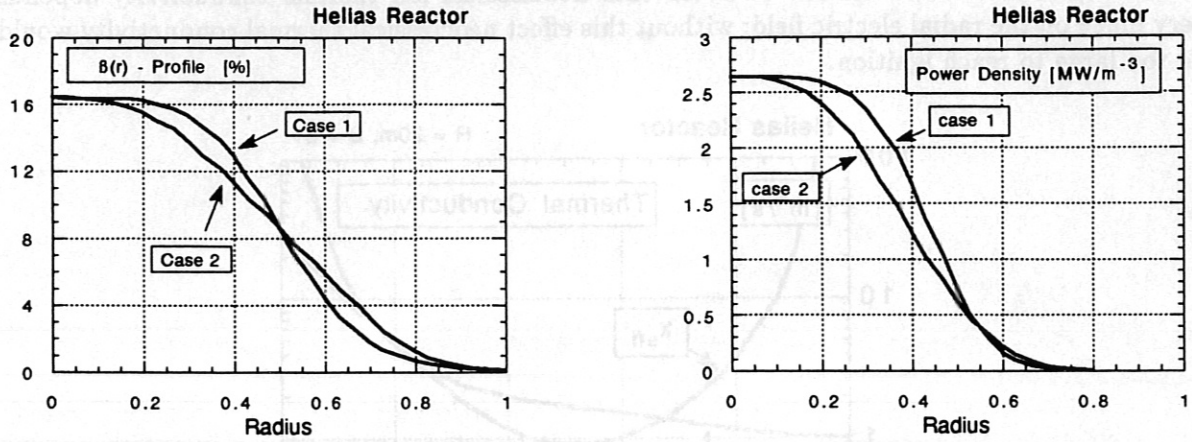

Figure 7: *β-profiles (left) and α-power density (right) in the Helias reactor*

3.3 Local Power Balance

In the ignited plasma the conductive heat losses must be balanced by the α-particle heating power $p_\alpha(r)$ minus radiation losses by bremsstrahlung $p_{br}(r)$. Since we have assumed equal temperature for all particle species, we obtain a simple relation for the thermal conductivities of ions and electrons which is

$$\chi_e + \chi_i = \frac{a^2 \int_0^r (p_\alpha - p_{br})\, r dr}{nr \frac{dT}{dr}} \tag{12}$$

This relation defines an upper limit on the thermal conductivity of a reactor plasma. The α-particle heating power has been calculated using the following form of the reaction rate [19]

$$< \sigma v > = 2.57 \cdot 10^{-18} \frac{\exp(-19.98(\frac{U}{T})^{1/3})}{T^{2/3} U^{5/6}} \tag{13}$$

where the function $U(T)$ is given by

$$U(T) = 1 - \frac{T(p_2 + (p_4 + p_6 T)T)}{1 + (p_3 + p_5 T)T} \tag{14}$$

The constants in this equation are $p_2 = 2.507 \cdot 10^{-2}, p_3 = 6.6 \cdot 10^{-2}, p_4 = 2.58 \cdot 10^{-3}, p_5 = 8.12 \cdot 10^{-3}, p_6 = -6.19 \cdot 10^{-5}$. The sum $\chi_i + \chi_e$ in Eq. 13 defines an upper limit on the thermal conductivity of reactor plasma. Using the α-heating power given in Eq. 13 this upper limit has been calculated. In Figure 8 this upper limit is shown as a function of the plasma radius. The mimimum value of χ_{eff} lies around 1 m/s^2; this number is rather invariant against parameter changes. For comparison the anomalous thermal conductivity of L-mode confinement is shown, this formula fits the L-mode confinement in the ASDEX tokamak [20]. To extrapolate this formula to a Helias reactor, a plateau-like scaling ($\propto 1/RB^2$) has been assumed.

$$\chi_{L-mode} = 1.5 \frac{1.6}{R} (\frac{2.2}{B})^2 \frac{T_e^{3/2}}{(1.1 - (r^2)^4} \quad [\frac{m^2}{s}] \tag{15}$$

An important result of this analysis is that the power balance in the Helias reactor is mainly dominated by the anomalous thermal conductivity; the neoclassical transport which was discussed in section 2.1 plays a minor role. Neoclassical transport coefficients of the Helias reactor are smaller

than $1m^2/s$. However, it should be noted that neoclassical ion thermal conductivity depends very much on the radial electric field; without this effect neoclassical thermal conductivity would be too large to reach ignition.

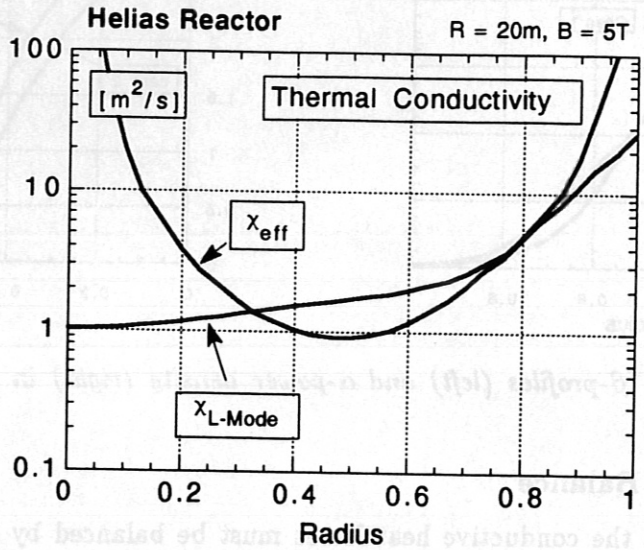

Figure 8: *Effective thermal conductivity in a Helias reactor from local power balance. Profile parameters:* r_T*=0.625,* r_n*=0.6,* α_T*=2.0,* α_n*=3.0*

3.4 Global Power Balance

In the following a power balance based on empirical scaling laws of anomalous confinement as described above will be discussed. Below the ignition threshold the plasma is maintained by an external heating power P_{ex} and the power balance is

$$\frac{E}{\tau_E} = P_\alpha + P_{ex} - P_{brems} \tag{16}$$

The right hand side is the available heating power which has to be inserted in the confinement time $\tau_E(B, \bar{n}, P...)$. Since the profiles are fixed this equation can be brought into the form

$$f(P_{ex}, n(0), T(0)) = 0 \tag{17}$$

Instead of $n(0), T(0)$ also the average values of n and T can also be used. The result of the power balance are presented in the form of the POPCON plots $P_{ex} = P_{ex}(n(0), T(0)) = \text{const}$. Several parameters have been varied to identify critical issues and possible solutions. These variations are:

- Two profiles: case 1 and case 2.
- Variation of impurity content: abundance of cold α- particles $\leq 10\%$, abundance of Oxygen $\leq 1\%$, abundance of Carbon $\leq 0.5\%$.
- Dependence on the isotope factor in τ_E, $A = 1.5 - 2.5$.
- Major radius 20 - 22m
- Magnetic field 5 - 5.5 T
- Confinement time: LHD scaling, Gyro-Bohm scaling and Lackner-Gottardi scaling.

The aim is to find an operating window where the ignited state (P_{ex} = 0) stays below the stability limit which is expected between $\bar{\beta}$ =4% and 5%. The lines $\bar{\beta}$ = 4% and $\bar{\beta}$ = 5% are also drawn on the POPCON plots. Such an operating window does not exist for confinement times following the Gyro-Bohm or the LHD- scaling; an improvement factor of 2 or less is needed. However, the Lackner-Gottardi scaling (LGS) predicts a higher confinement time and ignition can be reached without the need for further improvements. Therefore, only the results obtained with LGS will be presented in the following.

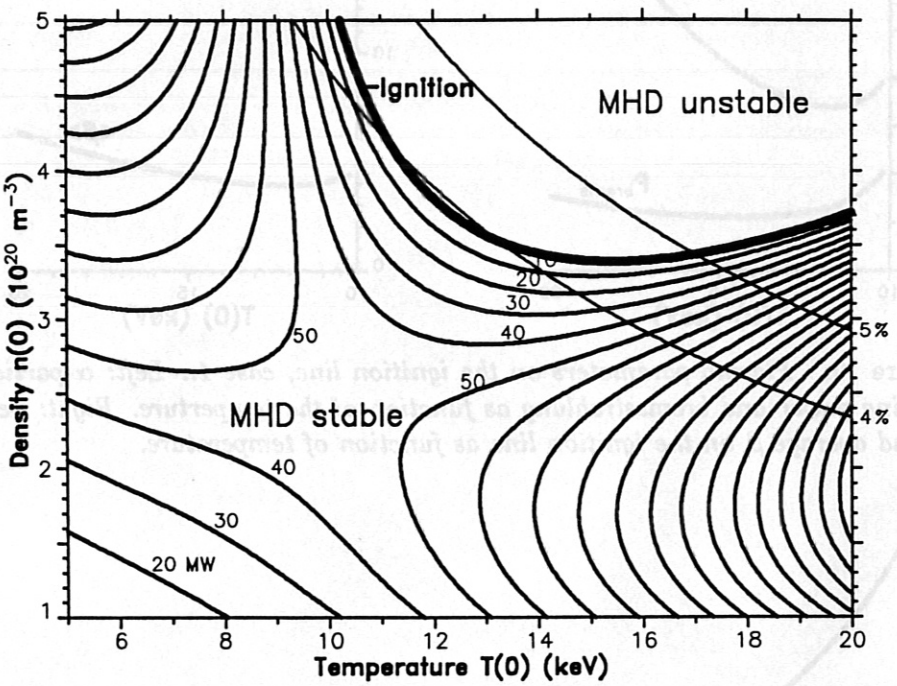

Figure 9: Contours of constant heating power, case 1. B=5 T,R=20 m f_α=10 %, LGS-scaling of confinement time, isotope effect included. Thick solid line: P_{ex}=0. Thin line indicate $\bar{\beta}$ =constant lines with $\bar{\beta}$=4% and 5%. Stability limit is defined by the ideal ballooning mode

In Figure 9 a rather optimistic case is shown: steep profiles (case 1) and an isotope effect in the τ_E-scaling are assumed. The maximum heating power is 50 MW; this power is needed to maintain the plasma at $n(0) - 2.5 \cdot 10^{20}$ m^{-3} and $T(0)$ = 11 keV. Going to higher density and temperature leads to a reduction of external heating power since α-particle heating begins to dominate. Finally, ignition can be reached at T = 12.5 keV and $n(0) = 3.8 \cdot 10^{20}$ m^{-3}. The average value of β is 4%. If the ignited state is thermally unstable, the temperature begins to increase until β reaches the stability limit and enhanced losses stabilize the burning state. In Figure 9 this could occur at $T(0)$ = 16 keV and $n(0) = 3.5 \cdot 10^{20}$ m^{-3}. The results show the strong dependence on the impurity content, the content of cold α-particles especially affects the fusion power output through the dilution effect. An amount of 10% α-particles and 1% carbon reduces the fusion power by roughly a factor of 2 at constant electron density. If the accumulation of cold α-particles is smaller (see the second and third column in Table II) the operating window lies below $\bar{\beta}$=4.5%.

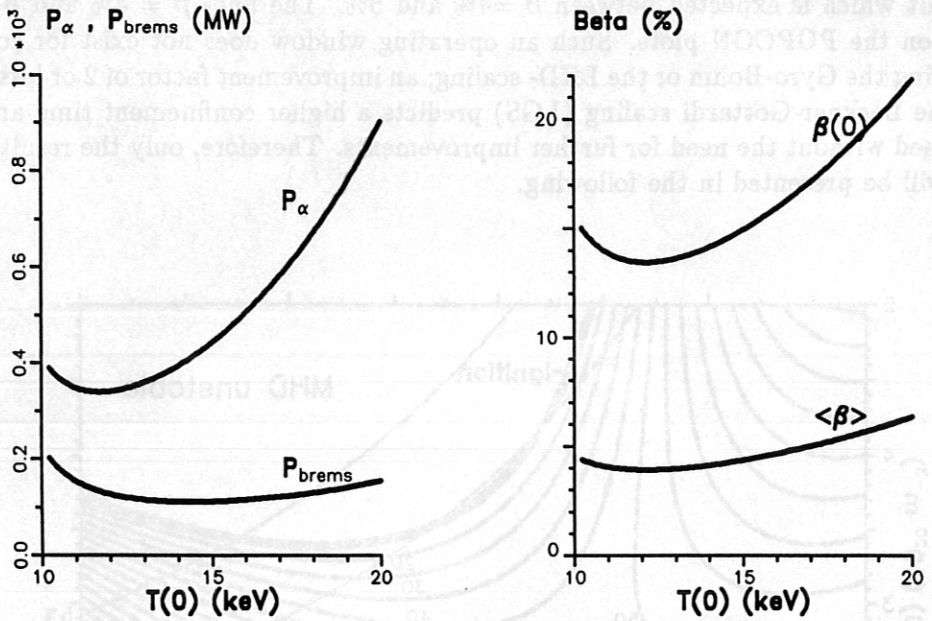

Figure 10: *Plasma parameters on the ignition line, case 1.. Left: α-particle heating power and bremsstrahlung as function of the temperture. Right: peak β and average β on the ignition line as function of temperature.*

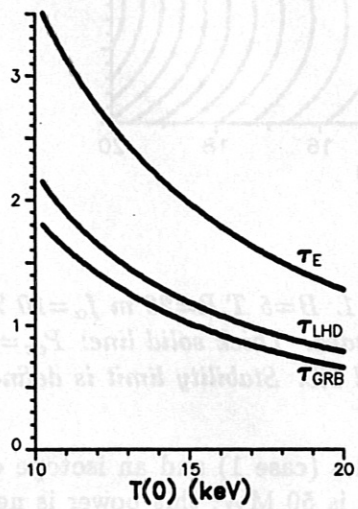

Figure 11: *Energy confinement time vs $T(0)$ on the ignition line. The top curve is the confinement time needed for ignition, it coincides with the LGS-time.*

Since the gradient of the plasma pressure is rather steep in the present choice of profile parameters a second case (case 2, see Figure 8) has been investigated where the pressure profile has been flattened. Reducing the pressure gradient raises the MHD-stability limit, the difference in pressure gradient between case one and case two is nearly a factor of 2. Furthermore, the isotope effect in the energy confinement time has been neglected, which yields a reduction of the confinement times by roughly 30%. Therefore, ignition is more difficult to achieve than under the optimistic assumption of case 1. The results listed in column 4 to 7 show that with a 10% increase of either the magnetic field or the overall size of the reactor keeping the magnetic field at 5T, the ignition condition can be met. If one increase the magnetic field to 5.5 T the peak field on the coils increase to more than 11 T and therefore NbTi- superconducting coils can no longer be used. This drawback is avoided with the option to increase the size of the device by 10%. A summary of the fusion power as a function of the average β is given in Figs. 12 and 13.

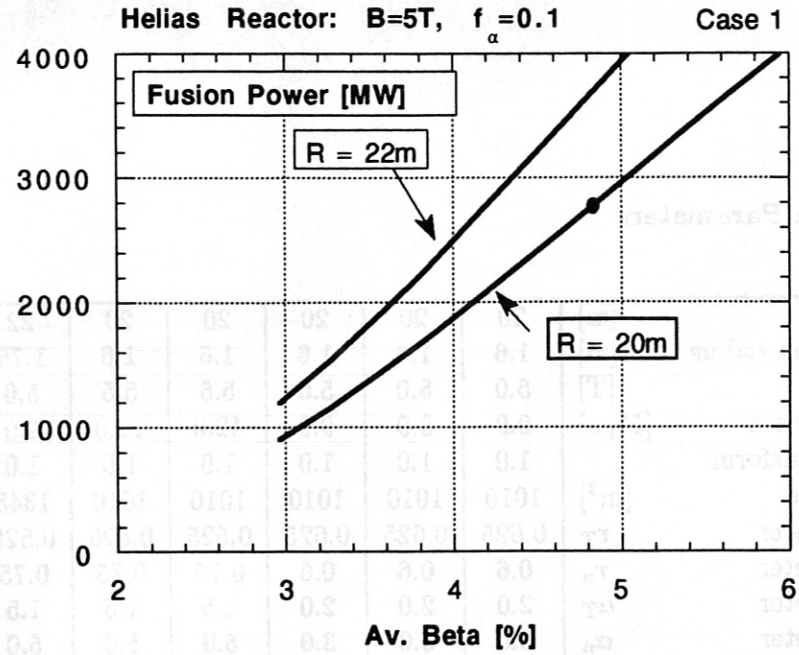

Figure 12: *Fusion power vs average β, case 1. $B = 5T$, $f_\alpha = 0.1$. The dot indicates the parameters listed in Table II, first column.*

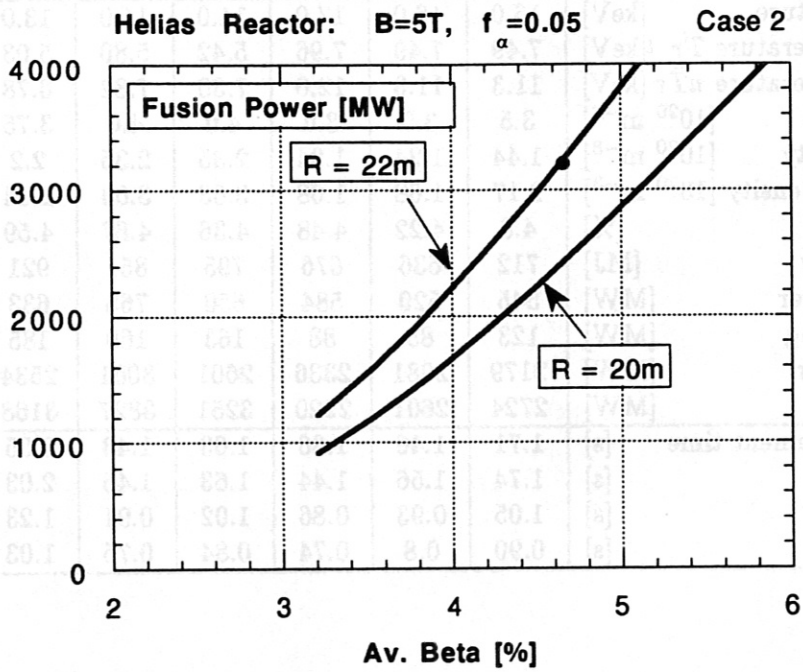

Figure 13: *Fusion power vs average β, case 2. $B = 5T$, $f_\alpha = 0.05$. The dot indicates the parameters listed in Table II, sixth column.*

Table II: Plasma Parameters

Major radius	[m]	20	20	20	20	20	22	22
Average plasma radius	[m]	1.6	1.6	1.6	1.6	1.6	1.76	1.76
Magnetic field	[T]	5.0	5.0	5.0	5.5	5.5	5.0	5.0
Magnetic pressure	[Mpa]	9.9	9.9	9.9	12.0	12.0	9.9	9.9
Rotational transform		1.0	1.0	1.0	1.0	1.0	1.0	1.0
Plasma volume	[m^3]	1010	1010	1010	1010	1010	1345	1345
Profile parameter	r_T	0.625	0.625	0.625	0.525	0.525	0.525	0.525
Profile parameter	r_n	0.6	0.6	0.6	0.75	0.75	0.75	0.75
Profile parameter	α_T	2.0	2.0	2.0	1.5	1.5	1.5	1.5
Profile parameter	α_n	3.0	3.0	3.0	5.0	5.0	5.0	5.0
Cold α-particles	f_α	0.1	0.05	0.05	0.05	0.05	0.05	0.05
Oxygen	f_{Oxygen}	0.01	0.01	0.01	0.005	0.005	0.005	0.05
Carbon	f_{Carbon}	0.001	0.001	0.001	0.001	0.001	0.001	0.001
Fraction of Hydrogen	n_H	0.714	0.814	0.814	0.854	0.854	0.854	0.854
Dilution factor		0.51	0.66	0.66	0.73	0.73	0.73	0.73
Z_{eff}		1.79	1.69	1.69	1.41	1.41	1.41	1.41
Peak temperature	[keV]	16.0	16.0	17.0	14.0	15.0	13.0	14.0
Average temperature $\bar{T}r$	[keV]	7.49	7.49	7.96	5.42	5.80	5.03	5.24
Average temperature $n\bar{T}r$	[keV]	11.3	11.3	12.0	7.30	7.82	6.78	7.30
Peak density	[10^{20} m^{-3}]	3.5	3.0	3.0	4.0	4.0	3.75	3.75
Average density	[10^{20} m^{-3}]	1.44	1.24	1.24	2.35	2.35	2.2	2.2
Average line density	[10^{20} m^{-3}]	2.17	1.68	1.68	3.03	3.03	2.84	2.84
Average beta	[%]	4.8	4.22	4.48	4.36	4.67	4.59	4.94
Plasma energy	[MJ]	712	636	676	795	851	921	991
α-heating power	[MW]	545	520	584	650	765	633	760
Bremsstrahlung	[MW]	123	85	88	163	169	185	192
Neutron power	[MW]	2179	2081	2336	2601	3061	2534	3042
Fusion power	[MW]	2724	2601	2920	3251	3827	3168	3803
Energy confinement time	[s]	1.71	1.46	1.36	1.63	1.43	2.05	1.74
τ_{LGS}	[s]	1.74	1.56	1.44	1.63	1.45	2.03	1.76
τ_{LHD}	[s]	1.05	0.93	0.86	1.02	0.91	1.23	1.07
$\tau_{Gyro-Bohm}$	[s]	0.90	0.8	0.74	0.84	0.75	1.03	0.89

4 Conclusions

As indicated in Section 2.1, the determining factors for the size of the Helias reactor are technical constraints and the large aspect ratio of the Helias configuration. The minimum size of the Helias reactor as listed in Table I is $R = 20$ m, and the estimated weight of the reactor core around 25000 tons. Given this size the minimum thermal power output should be around 3000 MW for economic reasons. As shown above, this requires an α-particle heating power of 500 MW. Since the fusion power is proportional to β^2 in this parameter regime, this requirement determines the minimum value of β. As has been shown, these β-values stay below 5% which is compatible with the MHD-stability limit against ideal ballooning modes. A $\bar{\beta}$ of 4 - 5% has not yet been achieved in stellarator experiments; the predictions above are based solely on theoretical arguements.

A similar situation exists in the issue of transport and plasma confinement. The neoclassical theory, which is well established, predicts transport coefficients well below the critical level of 1 m^2/s. Experiments in stellarators, however, exhibit anomalous confinement times smaller than neoclassical theory predicts. Since the underlying mechanism is unknown extrapolations to future experiments or to a Helias reactor are subject to some uncertainties. In extrapolating empirical scaling laws to a Helias reactor we have adopted a rather conservative point of view; improvement factors to meet the ignition condition have not been assumed, although arguments can be given that anomalous transport in Helias configurations might be smaller than in present-day stellarators or tokamaks. Although the Lackner-Gottardi scaling $\tau_E \propto Ra^2 B^{0.8} \bar{n}^{0.6} P^{-0.6} \iota^{0.4}$ is a so-called L-mode scaling, ignition in the Helias reactor can be reached, in contrast to tokamaks where L-mode confinement is not sufficient. Two reasons exist to explain this difference: one is the positive density scaling $\tau_E \propto \bar{n}^{0.6}$ and the absence of disruptive density limits in stellarators. Both effects have been verified in stellarator experiments. For this reason a Helias reactor can operate in a high-density regime ($n(0) = 2 - 4 \cdot 10^{20}$ m^{-3}) and at rather low temperatures ($T(0) \leq 16$ keV). Whether a radiative density limit will occur in a stellarator reactor is hard to forecast. Impurity accumulation depends very much on wall conditions and power load to the wall and divertor elements; this situation may be very different from present-day experiments, so that reliable predictions are impossible. The second effect which the Helias reactor makes profit of is the favourable scaling with the rotational transform ($\tau_E \propto \iota^{0.4}$) which yields a factor of 1 in HSR compared with $0.5^{0.4}$ in W 7-AS. Whether this effect really exists has still to be proven, experiments in Wendelstein 7-AS [15] exhibit a $\iota^{0.23}$-dependence of the confinement time(the parameter regime is $\iota \leq 0.6$). On the other hand the $\iota^{0.4}$-scaling is inferred from the banana orbit size in tokamaks and conventional stellarators. In Helias configurations , however, the particle orbits are quite different — the drift optimization leads to a reduction of the radial drift and reduces the size of banana orbits — and therefore a different ι-scaling may occur.

Furthermore, there is also the chance that H-mode confinement may exist in stellarators. Recently experiments in Wendelstein 7-AS showed H-mode like transitions in a currentless ECR-heated plasma [21] with improved confinement. This improvement of 20 - 30% is still small compared with the H-mode confinement in tokamaks, however, it already competes with the effect of the ion mass, the so-called isotope effect.

One difference in the three empirical scaling laws used above is the scaling with major radius R. Here the Lackner-Gottardi scaling has the strongest dependence ($\tau_E \propto R$). This — besides the ι-dependence— is the reason why the three scaling laws predict different results for the Helias reactor, although in present experiment the three scaling laws are nearly indistinguishable. Unfortunately, the three major existing stellarator experiments, W 7-AS, ATF and Heliotron E have nearly the same major radius — the difference is only 10% — and therefore it is left to future larger stellarators to decide upon the major radius scaling.

The isotope effect in τ_E yields an improvement factor of about 1.3. This effect, which has

been found in tokamak experiments, is not yet verified in stellarator experiments. Therefore, our analysis considered both cases; in Table III parameters of a Helias reactor are summarized where the confinement does not depend on the ion mass. Lackner-Gottardi scaling without the isotope effect still reaches ignition if the magnetic field is raised to 5.5 T or if the minor radius is increased to 1.8 m. In the first case the magnetic field on the coils also increases by 10% and NbTi-technology is no longer applicable. The second alternative leads to larger dimensions of the whole reactor core ($R = 20$ m, $a = 1.8$ m) and leaves the magnetic field at 5 T. These arguments underline the importance of the isotope effect and the need for an experimental clarification.

The reactor performance in a Helias reactor is strongly affected by dilution due to ash accumulation of thermal α-particles. Since the overall β-value is limited by MHD-instabilities any increase of impurity ions leads to a reduction of the deuterium and tritium content. In contrast to conventional stellarators, where prompt losses of highly energetic α-particles diminishes the α-heating power, these losses are strongly reduced in a Helias configuration by the poloidal magnetic drift. Highly energetic and trapped α- particles are confined for one slowing-down time, which is enough to contribute to plasma heating. A longer confinement time of α- particles is not desired since this would favour the accumulation of thermal α-particles. The neoclassical confinement time of thermal α-particles in the Helias reactor has been estimated to be around 15 s, which is less than 10 energy confinement times. This suggests that the abundance of thermal α-particles might stay below 10%; in our analysis $f_\alpha = 10\%$ has been assumed as the maximum value. Furthermore, it should be noted that present stellarator experiments exhibit anomalous particle transport which is roughly a factor of 5-10 slower than energy transport. If this persists in a reactor then anomalous transport of thermal α-particles is to be expected. Another argument is the enhanced transport close to the β-limit. If the thermal instability of the reactor is stabilised by the MHD- stability limit, this implies enhanced transport processes in the burning plasma, an enhanced particle transport similar to tokamak discharges with sawtooth oscillations is to be expected. In this context the absence of a pinch effect in stellarators should also be very helpful to reduce the level of impurities and helium ash. Present stellarator experiments do not show a pinch effect and for theoretical reason a neoclassical pinch effect vanishes if the bootstrap effect is zero. The specific choice of the magnetic configuration in the Helias reactor was determined by the constraint of zero bootstrap current and therefore zero pinch effect follows from the Onsager conjugacy of these two effects.

The preceeding analysis has shown that the state of the burning plasma is determined by anomalous transport processes rather than by neoclassical transport. If this anomaly follows the LHD scaling or the Gyro-Bohm scaling the confinement time is a factor of two too small to reach ignition. If the confinement time follows the Lackner-Gottardi scaling, this L-mode like confinement is sufficient for ignition. Once ignition is reached the onset of MHD-instabilities — expected in the range $\bar{\beta} = 4$-5% — will enhance the plasma transport and thus determine the burn point. These MHD-instabilities certainly will have some effect on the particle transport and therefore also affect the accumulation of impurities and Helium ash. In many respects the power balance in the Helias stellarator is similar to that in a tokamak reactor, except for the absence of a disruptive density limit which allows one to run the reactor at high density, $\bar{n} \geq 2 \times 10^{20} \mathrm{m}^{-3}$, and low temperature. In this case one gains from the favourable scaling of the confinement time with density which is found in stellarator experiments.

References

[1] R.L. MILLER,R.A. KRAKOWSKI *Proceedings of the 3rd Technical Committee Meeting and Workshop on Fusion Reactor Design and Technology*, Tokyo, Japan, 1981, IAEA-TC-392/20, Vienna 1983, Vol. I, 343.

[2] G. GRIEGER, E. HARMEYER, J. KIßLINGER, F.RAU, H. WOBIG *Proceedings of the 4th Technical Committee Meeting and Workshop on Fusion Reactor Design and Technology*, Yalta, USSR, 1986, IAEA I3-TC-392.3/21, Vienna 1987, Vol. I, 341.

[3] J. NÜHRENBERG, R. ZILLE, *Phys. Letters* A **114** (1986) 129

[4] C.D. BEIDLER, G. GRIEGER, E.HARMEYER, N. KARULIN, J. KIßLINGER, W. LOTZ, J. NÜHRENBERG, F. RAU, H. WOBIG *Proc. of the 14th Int. Conf. on Plasma Physics and Controlled Nuclear Fusion Research*, Würzburg, BRD, 1992, IAEA-CN56/G-I-2, Vienna.(to be published)

[5] M. MURAKAMI et al 1991 *Proc. of the 13th IAEA Conf. on Plasma Phys. and Contr. Nucl. Fus. Res.* Vienna vol 2 455

[6] V. ERCKMANN, H. GASPARINO,H. MAAßBERG, 1992 *Plasma Phys. and Contr. Fusion* vol **34** 1917

[7] K. LACKNER, N.A.O. GOTTARDI, *Nucl. Fusion* **30** (1990) 767

[8] W. LOTZ, P. MERKEL, J. NÜHRENBERG, E. STRUMBERGER *Plasma Phys. and Contr. Fusion* **34** (1991), 1037

[9] C.D. BEIDLER, G.GRIEGER, F. HERRNEGGER, E. HARMEYER, J. KIßLINGER, W. LOTZ, H. MAßBERG, P. MERKEL, J. NÜHRENBERG, F. RAU, J. SAPPER, F. SARDEI, R. SCARDOVELLI, A. SCHLÜTER, H. WOBIG, *Fusion Technology* **17** (1990) 148

[10] J. KIßLINGER, H. WOBIG, *Europhysics Conf. Abstracts* Vol. 9F, Part I, (1985) 453

[11] E. HARMEYER, J. KIßLINGER, F. RAU, H. WOBIG, IPP-Report 2/316, Feb. 1993

[12] LOTZ, W., NÜHRENBERG, J., *Phys. Fluids* **31**, (1988) 2984.

[13] HIRSHMAN, S.P., SHAING, K.C., VAN RIJ, W.I., BEASLEY, C.O., Jr.,CRUME, E.C., Jr., *Phys. Fluids* **29**, (1986) 2951.

[14] C.D. BEIDLER, *18th European Conf. Controlled Fusion and Plasma Physics* (Proc. 18th Int. Conf. Berlin, Germany, 1991), Vol. 15C, Part II, (1991) 177.

[15] H. RENNER et al. *Proc. of the 13th IAEA Conf. on Plasma Phys. and Contr. Nucl. Fus. Res.* Vienna vol 2 439

[16] M. MURAKAMI et al. *Proc. of the 14th Int. Conf. on Plasma Physics and Controlled Nuclear Fusion Research*, Würzburg, BRD, 1992, IAEA-CN56/.., Vienna.(to be published)

[17] H.E. MYNICK, Princeton Plasma Physics Laboratory Report, PPPL-2658 (1992)

[18] R. BEHRISCH, V. PROZESKY, *Nuclear Fusion* **30** (1990) 2166.

[19] G. SADLER, P. VAN BELLE, JET-report JET-IR(87)08, 1987

[20] K. LACKNER et al. *Plasma Physics and Contr. Fusion* **31** No. 10, (1989) 1629

[21] V. ERCKMANN et al. *Proc. of the 14th Int. Conf. on Plasma Physics and Controlled Nuclear Fusion Research*, Würzburg, BRD, 1992, IAEA-CN56/.., Vienna (to be published)